



# Characterization of atmospheric methane release in the outer Mackenzie River Delta from biogenic and thermogenic sources.

Daniel Wesley<sup>1,2</sup>, Scott Dallimore<sup>3</sup>, Roger MacLeod<sup>3</sup>, Torsten Sachs<sup>4</sup>, David Risk<sup>1</sup>

<sup>1</sup>Department of Earth Science, St. Francis Xavier University, Antigonish, B2G 2W5, Canada

5 <sup>2</sup>Department of Environmental Science, Memorial University, St. John's, A1C 5S7, Canada

<sup>3</sup>Geological Survey of Canada-Pacific, Natural Resources Canada, Sidney, V8L 4B2, Canada

<sup>4</sup>GFZ German Research Centre for Geosciences, Telegrafenberg, 14473 Potsdam, Germany

*Correspondence to:* Daniel Wesley (dwesley@stfx.ca)

**Abstract.** The Mackenzie River Delta is the second largest Arctic river delta in the world. Thin and destabilizing permafrost  
10 coupled with vast natural gas reserves at depth, high organic content soils, and a high proportion of wetlands create a unique  
ecosystem conducive to high rates of methane (CH<sub>4</sub>) production from biogenic and thermogenic sources. Hotspots are known  
to have a significant contribution to summertime CH<sub>4</sub> emissions in the region, but little research has been done to determine  
how often geologic or biogenic CH<sub>4</sub> contributes to CH<sub>4</sub> hotspots in the Mackenzie River Delta. In the present study, stable  
15 carbon isotope analysis was used to identify the source of CH<sub>4</sub> at several aquatic and terrestrial sites thought to be hotspots of  
CH<sub>4</sub> flux to the atmosphere. Source stable carbon isotope ( $\delta^{13}\text{C-CH}_4$ ) signatures were derived from keeling plots of point  
samples and ranged from -42 to -88 ‰  $\delta^{13}\text{C-CH}_4$ , identifying both biogenic and thermogenic and mixed biogenic/thermogenic  
sources. A CH<sub>4</sub> source was determined for eight hotspots, two were thermogenic in origin, four were biogenic in origin, and  
two were from mixed biogenic/thermogenic sources, as evidenced by  $\delta^{13}\text{C-CH}_4$  signatures. This indicates that the largest  
20 hotspots of CH<sub>4</sub> production in the Mackenzie River Delta are caused by a variety of sources. In addition to biogenic production  
at the surface we have identified CH<sub>4</sub> migration to the surface from the Taglu gas field over an area of approximately 20 km  
from north to south and two different sites of mixed biogenic/thermogenic CH<sub>4</sub> that were approximately 30 km apart.

## 1 Introduction

The Mackenzie River Delta (MRD) in the western Canadian Arctic is a unique setting for environmental methane (CH<sub>4</sub>)  
emission to the atmosphere. Geological CH<sub>4</sub> occurs at depth and within shallow surficial sediments, and there are many diverse  
25 settings in the area where biogenic methane production is actively occurring. The area is characterized by thin and destabilizing  
permafrost (Burn and Kokelj, 2009), high organic content soils (Schuur et al., 2008), vast amounts of deep thermogenic  
methane (Collett and Dallimore, 1999) and over 49,000 lakes which make up 25 - 50 % of the landscape (Emmerton et al.,  
2007; Lewis, 1988; Mackay, 1963). Importantly, atmospheric release of CH<sub>4</sub> during the summer in the MRD is thought to be  
characterized by localized areas with high methane flux, or 'hotspots' (Kohnert et al., 2017). Due to the potential for large



30 contributions of geologic CH<sub>4</sub> and conditions conducive for biogenic CH<sub>4</sub> production, it is important to understand these sources of CH<sub>4</sub> emissions, especially in areas of high-rate emissions.

Studies of atmospheric methane flux in the Arctic suggest that there are several factors that can influence methane dynamics in terrestrial and aquatic settings. These include, environmental controls such as vegetation type, oxygen availability, soil moisture and soil temperature (including active layer regime) which can affect CH<sub>4</sub> and CO<sub>2</sub> production, transport, and emissions (Rawlins et al., 2010; Treat et al., 2018). In addition, ecosystem heterogeneity can cause large variation in these environmental controls, all of which will be impacted by climate change (Collins et al., 2013). The MRD is characterized by a high proportion of wetlands and shallow tundra lakes (Ecosystem Classification Group, 2009, 2012;). Wetlands are considered to be the largest natural source of CH<sub>4</sub> globally, and wetland emissions are predicted to increase worldwide (Dean et al., 2018). Current global estimates of wetland CH<sub>4</sub> flux to the atmosphere range between 153-227 Tg CH<sub>4</sub>/yr (Saunois et al., 2016). Non-wetland, freshwater systems are also significant contributors of CH<sub>4</sub> to the atmosphere on a global scale (Kirschke et al., 2013) which is estimated between 60-180 Tg CH<sub>4</sub>/yr (Saunois et al., 2016). Ebullition from sediments is one path for CH<sub>4</sub> to enter the atmosphere from freshwater bodies (Saunois et al., 2016). In fact, a recent study showed that despite substantial winter-derived CH<sub>4</sub> being retained in bottom waters of a lake in the MRD due to ice cover, CH<sub>4</sub> migrated to the atmosphere during the open water period (McIntosh Marcek et al., 2021). Emissions from thermokarst water bodies, such as those in the MRD, are expected to increase in the future due to longer annual ice-free periods (Wik et al., 2016; Marsh, 1990). Moreover, lakes (Kohnert et al., 2018), and natural seeps of thermogenic CH<sub>4</sub> (Bowen et al., 2008; Kohnert et al., 2017) are known sources of CH<sub>4</sub> in the MRD.

Determining the ratio of <sup>13</sup>C/<sup>12</sup>C or stable carbon isotope ratio ( $\delta^{13}\text{C-CH}_4$ ) is one of the most established methods to assess CH<sub>4</sub> sources to the atmosphere. Globally, atmospheric CH<sub>4</sub> has a background stable carbon isotope ratio of approximately -47 ‰ (Allan et al., 2001; Nisbet et al., 2016). Biogenic sources are depleted in <sup>13</sup>C and therefore have a lower (lighter) stable carbon isotope ratio, whereas thermogenic sources are enriched in <sup>13</sup>C and have a higher (heavier)  $\delta^{13}\text{C-CH}_4$  (Brownlow et al., 2017). However, thermogenic signatures in particular can vary significantly, even within the same field, as they are influenced by the source rocks and formation processes (Schoell, 1980). While there have been numerous hydrocarbon exploration wells drilled in the MRD area, we are only aware of information on thermogenic  $\delta^{13}\text{C-CH}_4$  values for reservoirs of the Taglu gas field which vary from -25 to -50 ‰ for multiple gas horizons at depths from 1700 to > 4000 m depth (Collett and Dallimore, 1999). Similar to these authors, we consider isotopic values > -50 ‰ to indicate thermogenic sources while values < -70 ‰, indicate biogenic CH<sub>4</sub>. Intermediate values may indicate gases which is a mixture of biogenic and thermogenic CH<sub>4</sub>. Although complexities can result from geochemical processes such as CH<sub>4</sub> oxidation which can change the  $\delta^{13}\text{C-CH}_4$  due to a preference for bacteria to oxidize CH<sub>4</sub> containing the lighter isotope enriching the remaining CH<sub>4</sub> with <sup>13</sup>C.

60 Migration of CH<sub>4</sub> through discontinuities in the permafrost is common in the MRD as well as production in the organic rich active layer. Previous work has shown that thermogenic (Bowen et al., 2008; Walter Anthony et al., 2012; Walter et al., 2006) and biogenic (Zona et al., 2016; Walter Anthony et al., 2010) hotspots are present in Arctic permafrost environments, and suggest that both are present in the outer MRD (Kohnert et al., 2018). The Arctic is experiencing rapid



climate change, soil temperatures are increasing in the outer MRD (Burn and Kokelj, 2009), permafrost is warming in the  
65 Canadian Arctic (Farquharson et al., 2019; Mamet et al., 2017) and globally (Biskaborn et al., 2019). Talik formation is  
common below lakes in the MRD (Burn, 2002) and will increase with permafrost thaw. This will provide the means for greater  
CH<sub>4</sub> release from thermogenic and biogenic sources in the MRD in the future. Therefore, it is important to continue to measure  
emissions of CH<sub>4</sub> in the rapidly changing environment of the MRD.

Due to the varied thermogenic and biogenic CH<sub>4</sub> sources in the MRD it is important to determine the contribution of  
70 each source to the atmosphere as a basis to appraise carbon budgets. A lack of understanding of CH<sub>4</sub> sources in the MRD could  
lead to underestimation of permafrost greenhouse gas emissions in the region and assessments of changes that could occur  
from ongoing and future climate change. To date, very little research has been done to appraise geologic vs biogenic CH<sub>4</sub>  
contributions both at a regional scale and for hotspots with concentrated atmospheric flux. A recent study by Kohnert et al.  
(2017) found that about 1% of the mapped area in the outer MRD was an extremely high source of CH<sub>4</sub> with flux rates above  
75 5 mg m<sup>-2</sup> h<sup>-1</sup>. These authors assumed that these hotspots were primarily of geologic origin since the inferred flux rates of the  
hotspots identified were significantly greater than the maximum published value for biogenic fluxes north of 61°N (Friborg et  
al., 2000; Sturtevant et al., 2012; Sachs et al., 2008) and they occurred in the summer period when most lakes were fully  
oxygenated, reducing biogenic emissions. Importantly, isotopic signatures have not been extensively used to determine the  
source of atmospheric CH<sub>4</sub> at hotspots in the outer MRD and these sources could behave differently than the current  
80 understanding of the region and other, similar Arctic environments.

The goal of this study is to undertake a first appraisal of the source of CH<sub>4</sub> from hotspots in the MRD with varied  
geology and permafrost conditions as identified by Kohnert et al (2017). This research objective will be addressed by  
measuring the stable carbon isotope ratio of atmospheric methane emissions to determine if they were from possible  
thermogenic or biogenic sources. We hypothesise that the largest hotspots in the MRD include contributions from both  
85 thermogenic, biogenic and mixed sources due to the complex nature of potential geologic CH<sub>4</sub> sources at depth in the region  
and the abundance of environmental settings where modern methane is being produced.

## 2 Setting

The MRD is the second largest Arctic river delta in the world and the largest river delta in Canada (Walker, 1998). It occurs  
between the higher elevation Pleistocene deposits of the Yukon coastal plain to the west and the Tuktoyaktuk coastlands to the  
90 east. The subaerial delta is thought to have formed in a glacial valley filled with late Pleistocene glacial sediments that were  
subsequently overlain by Holocene-aged deltaic deposits (Hill et al., 2001). A succession of Tertiary-aged hydrocarbon bearing  
sediments occurs at depth beneath the entire MRD region with a number of large thermogenic hydrocarbon fields being  
identified by industry (Osadetz and Chen, 2010). Deltaic sediments occurring in the near surface consist mainly of fine sand  
and coarse silts which are >100 m thick in the most of the MRD, but can be less than 20 m thick in the extreme north-eastern  
95 areas (Dallimore et al, 1992; Mackay, 1963). Permafrost is considered to be continuous beneath land areas, but is largely absent



beneath lakes which do not freeze to the bottom in winter (Nguyen et al., 2009). Ground ice content in deltaic sediments may exceed 50% in near surface sediments, but is substantially lower at greater depths (Collett and Dallimore, 1999; Mackay, 1963). Ground ice exists in the form of bonding cement or visible ice in excess of the pore space occurring as lenses, veins and rarely as massive ice layers (>1m in thickness).

100 The MRD has a variety of unique permafrost landforms including extensive areas with ice wedge polygons and a  
number of isolated pingos which can range in size from just a few metres to 10-20 m high (Mackay, 1963; Wolfe et al., 2021).  
Bowen et al. (2008) has also identified a number of pock mark features in water bodies that are thought to be caused by  
geologic methane flux. The outer MRD is experiencing the ongoing effects of climate change (Burn and Kokelj, 2009), rapid  
coastal retreat and warming air temperatures that have risen in the past three decades at a rate that is three times the global  
105 average (GRID-Arendal, 2020).

### 3 Methods

In the present study, we investigated several aquatic and terrestrial hotspots of atmospheric CH<sub>4</sub> flux. Study sites visited in the  
summer were chosen based on areas with high methane flux rates determined from airborne eddy covariance flux surveys,  
conducted in the outer MRD by the German Research Centre for the Geosciences (GFZ) together with the Alfred Wegener  
110 Institute for Polar and Marine Research (AWI) (Kohnert et al., 2017). We conducted ground sampling surveys in July 2019  
and 2021. The airborne eddy covariance flux surveys were conducted seven years prior, during the same month in 2012 and  
2013. We also carried out fieldwork in October of 2019 focussing on sampling near holes in the ice forming on water bodies  
caused by high rate CH<sub>4</sub> ebullition.

#### 3.1 Study Location

115 The study sites are shown in Fig. 1 and are superimposed on a map of concentrated areas with high CH<sub>4</sub> flux rates derived  
from published results by Kohnert et al. (2017). Eight of the nine study sites were located within the MRD and one site was  
located within the Tuktoyaktuk coastlands. Five study sites were located at large (about 1-5 km<sup>2</sup>), but well-defined hotspots  
with methane flux rates, determined from aerial surveys by Kohnert et al. (2017) to be in excess of 5 mg hr<sup>-1</sup>m<sup>-2</sup> (Pingo 1,  
Pingo 2, Wetland 2, Wetland 3, Site 9). Of the five airborne eddy covariance hotspots investigated, atmospheric CH<sub>4</sub>  
120 concentrations were significantly above background at four sites (Pingo 1, Pingo 2, Wetland 2, Wetland 3). Only background  
atmospheric concentrations of CH<sub>4</sub> were observed at Site 9 (Table S1), therefore, it was not included in the main analysis. Site  
9 was a tundra site vegetated mainly with shrub willows and alders. Walking transects were conducted at all of these sites due  
to their large and areal nature in order to increase sampling coverage. Discrete point samples were taken at each site for stable  
carbon isotope ratio ( $\delta^{13}\text{C-CH}_4$ ) determination.

125 Four additional sites (Pingo 3, Wetland 1, Lake 1, Channel Seep) were at locations where aquatic seeps with focussed  
CH<sub>4</sub> flux was observed as ebullitions seen in open water in summer, or in holes in newly formed ice in the fall. Discrete point



130 samples were taken for stable carbon isotope ratio ( $\delta^{13}\text{C}\text{-CH}_4$ ) analysis. Point samples were taken as close as possible to observed ebullitions with additional samples taken up to 5 m away from known sources in order to measure source and background  $\text{CH}_4$  concentrations. Walking transects and discrete point samples were completed at Pingo 3 and Wetland 1 in the summer of 2021 to compare overall site variation to point source samples.

135 The main study sites were situated in the lower subaerial delta plain which consists of deltaic sediments, many meandering river channels and numerous thermokarst lakes (Burn and Kokelj, 2009). The permafrost in this area is typically less than 100 m thick and continuous beneath land areas (Nguyen et al., 2009). However, taliks, or thawed zones in the permafrost, form below most lakes and channels and often penetrate the entire permafrost interval (Burn, 2005). The high number of lakes in the area is characteristic of many Arctic and Subarctic deltas (Marsh, 1990). In the outer MRD, lakes tend to remain oxygenated and have well established macrophyte communities by the end of the summer (McIntosh Marcek et al., 2021). Many of the lakes are isolated from the flow of the channels of the Mackenzie River, except during storm surge inundation (Marsh, 1990). Terrestrial areas are dominated by mixed tundra vegetation with some areas (particularly along the edge of river channels) with well-developed shrub willow and alders, however other areas are more sparsely vegetated with exposed delta muds and sedge vegetation (Burn and Kokelj, 2009; Gill, 1972). Many flat-lying terrestrial areas are covered by 140 10-40 cm of standing water during late summer. Since all sites were only accessible by helicopter, field access was largely dependent on weather and ground conditions at each site.

Pingo 3 is located to the east of the MRD in an area referred to as the Tuktoyaktuk coastlands (Ecosystem Classification Group, 2012). This site was sampled in the fall in a shallow pond which formed in the crater of a collapsed 145 pingo. Steady ebullition of  $\text{CH}_4$  occurring in the pond maintained open holes in newly formed ice. This site is located east of the airborne eddy covariance flux surveys conducted by Kohnert et al. (2017) (Fig. 1). The surficial materials in this area were characterized by glacial moraine with continuous shrub tundra vegetation. However, the pingo itself was located in a drained lacustrine basin and similar to many other pingos in the Tuktoyaktuk coastlands area in general (Ecosystem Classification Group, 2012). Permafrost Tuktoyaktuk coastlands typically is more than 400 m thick and therefore through going taliks are 150 much more rare.

### 3.2 Sample Collection

Geolocated air samples were collected in the field and subsequently analysed at the Aurora Research Institute laboratory in Inuvik, NWT, Canada or at St. Francis Xavier University in Antigonish, NS, Canada.  $\text{CH}_4$  and  $\text{CO}_2$  concentrations and  $\delta^{13}\text{C}\text{-CH}_4$  were determined using a Picarro G2210i analyser. Sample positions were recorded with a handheld GPS. Five walking 155 transects of atmospheric  $\text{CH}_4$ , and  $\text{CO}_2$  concentrations were completed at Pingo 1, Pingo 2, Wetland 2, Wetland 3, and Site 9 in 2019 (Fig. 1). Hotspots determined by airborne eddy covariance were typically several square kilometres in extent and therefore it was impractical to sample the entire feature. Sampling transect locations were selected within the general hotspot area focussing on wetland areas or pingos that were considered possible sources of  $\text{CH}_4$ . Photographs of each site and descriptions are included in Fig. 2. Walking transects were carried out by filling a 30 m coil of 6 mm aluminium Synflex tubing



160 at a constant rate while walking at a steady pace across the ground or by carrying a Li-Cor LI-7810 gas analyser. Five walking  
transects using Synflex tubing took approximately 20 minutes to fill and covered a distance between 600-800 m. Analytical  
determinations made at a regular spacing on the tubing allowed for consideration of spatial variability in methane  
concentrations. Mixing between sample collection and analysis is limited due to the small diameter of the tubing. A similar  
method was used during drone-based CH<sub>4</sub> measurements (Andersen et al., 2018). Two walking transects were collected at  
165 Pingo 3 and Wetland 1 in 2021 using a Li-Cor LI-7810 gas analyser over an approximately 10 minute period and covered a  
distance of approximately 200-300 m. Sample air was drawn from approximately 1 m above ground level.

Discrete point samples were taken at all sites by filling 1 L Tedlar bags with ambient air from approximately 1 m  
above ground level. At aerial eddy covariance sites point samples were taken along each walking transect. The point samples  
were used to measure stable carbon isotope ratios ( $\delta^{13}\text{C-CH}_4$ ). Wind regime at sample sites was measured with a Kestrel 1000  
170 handheld anemometer which has an accuracy of +/- 0.1 m/s.

Flux chamber measurements were taken at Pingo 3 using a Li-Cor LI-7810 with an automated chamber and at Lake  
1 site using manual extraction of samples because the soil was too wet to use the automated chamber. The flux chamber  
consisted of a cylindrical chamber with a height of 33 cm and a diameter of 25 cm. Collars for the manual and automated soil  
chambers were installed at least 1 hour before flux measurements were taken. Vials of air were drawn from the middle of the  
175 chamber at 10-minute intervals using a syringe and were analysed on a Shimadzu GC-14B gas chromatograph for CH<sub>4</sub> and  
CO<sub>2</sub>.

### 3.3 Determination of CH<sub>4</sub> Source Stable Carbon Isotope Ratio ( $\delta^{13}\text{C-CH}_4$ )

Keeling plots analysis of the discrete point samples was used to determine the stable carbon isotope signature of the CH<sub>4</sub> source  
at each site. Keeling plot analysis is a common approach used to determine a source of carbon entering the atmosphere by  
180 measuring the change in  $\delta^{13}\text{C-CH}_4$ , or fractionation, that occurs as more carbon from that source is added (Kohler et al., 2006).  
This analysis uses a mass balance approach and takes into account the relative difference in stable carbon isotope ratios of the  
atmosphere and an additional carbon source (Kohler et al., 2006; Pataki et al., 2003). The Y intercept of a linear regression of  
the  $\delta^{13}\text{C-CH}_4$  vs. the inverse of the CH<sub>4</sub> concentration will indicate the source which contributed the increase in atmospheric  
CH<sub>4</sub>. This approach was first used by Keeling (1958, 1961) to determine the source of CO<sub>2</sub> contributions to the atmosphere  
185 (Pataki et al., 2003). One main assumption of Keeling plot analysis is that there are only two components being measured, the  
source being released at the surface/atmosphere interface and the background regional atmospheric signature (Pataki et al.,  
2003). This assumption is challenging to achieve under field conditions as there can be multiple potential sources of CH<sub>4</sub> if  
the sampling is carried out over a broad area or in windy conditions that may cause mixing. For the walking transects described  
in our study, we accepted this limitation as we were attempting to appraise rather large hotspots identified by Kohnert et al.  
190 (2017). On this basis, it seemed reasonable to accept that our atmospheric point samples, conducted within the assumed source  
of these six hotspots, could be representative of a blended  $\delta^{13}\text{C-CH}_4$  signature as might be measured by these researchers at  
the elevation that the survey aircraft was flying (40-80 m above ground level). In comparison, at sites where ebullition was





observed and there was a known point source of emission, an attempt was made to sample as close as possible to that source. This enables a high degree of certainty that only one source is being measured at Pingo 3, Wetland 1, Lake 1, and Channel Seep sites.

## 4.0 Results

Data obtained from walking transects at each site are compiled with wind speed in Table 1. Atmospheric CH<sub>4</sub> concentrations were elevated at four of five sites where walking transects were completed at airborne eddy covariance hotspot sites. Mean background atmospheric values recorded at the Inuvik ECCC weather station for the period of fieldwork (July 8-19, 2019) were 1.995 ppm for CH<sub>4</sub> and 402 ppm CO<sub>2</sub>. The maximum CH<sub>4</sub> values for walking transects obtained were 8.734 ppm at Pingo 2, 6.135 ppm at Pingo 1, 2.264 ppm at Wetland 3, 2.152 ppm at Wetland 2, and background values at Site 9. Elevated CO<sub>2</sub> values were also observed during walking transects at two of the eddy covariance hotspot sites with values of 603 ppm at Wetland 2 and 463 ppm at Pingo 2. Estimates of source stable carbon isotope signatures ( $\delta^{13}\text{C-CH}_4$ ) derived from Keeling plots were 53.0 ‰ for Pingo 1, -63.6 ‰ for Pingo 2, -78.4 ‰ for Wetland 2, and -71.9 ‰ for Wetland 3.

As expected, the four sites with discrete samples in close proximity to ebullition sites had substantially elevated methane concentrations (Fig. 1). Estimates of source stable carbon isotope signatures derived from Keeling plots (Fig. 3) were -77.6 ‰ for Pingo 3, -42.5 ‰ for Channel Seep and -44.7 ‰ for Lake 1. Keeling plot values were -88.4 ‰ for Wetland 1 when sampled in the fall, but -56.7 ‰ when sampled in the summer. Pingo 3, and Lake 1, and Wetland 1 were sampled in the fall with ebullitions forming holes in the newly formed ice. Channel Seep was documented during a previous field campaign. Maximum values of 2.94 ppm CH<sub>4</sub> and 519 ppm CO<sub>2</sub> were observed at Pingo 3 and values of 12.399 ppm CH<sub>4</sub> and 488 ppm CO<sub>2</sub> were observed at Wetland 1. Flux rates for CH<sub>4</sub> and CO<sub>2</sub> were measured in 2021 at Lake 1 and Pingo 3 (Table S2).

## 5 Discussion

### 5.1 Methane characteristics observed at airborne eddy covariance hotspot sites

#### Outer delta pingos

The highest CH<sub>4</sub> values for walking transects co-located within airborne eddy covariance CH<sub>4</sub> hotspots were obtained in the north-western part of the outer MRD. Maximum CH<sub>4</sub> concentrations of 8.734 ppm were observed at Pingo 2 with elevated concentrations above 2.5 ppm were observed for 285 of 2013 observations during the walking transects. Maximum concentrations of 6.135 ppm were observed at Pingo 1 with values above 2.5 ppm were observed for 1056 of 1850 observations during the walking transects. The elevated values observed over a dispersed area within the eddy covariance hotspots provides a basis to speculate on the possible sources for the hotspots. Estimates of source stable carbon isotope signatures ( $\delta^{13}\text{C-CH}_4$ ) derived from Keeling plots were -53.0 ‰ for Pingo 1 and -63.6 ‰ for Pingo 2 with reasonable confidence in these



determinations as they were derived with multiple isotopic measurements for each Keeling plot. These signatures are substantially enriched in  $^{13}\text{C}$  compared to typical biogenic sources and relatively close to our assumed threshold of -50 ‰ based on thermogenic gas found in the Taglu hydrocarbon reservoir. We conclude, therefore, a geologic source for the methane for each site is made up of a mixture of thermogenic and biogenic gas from depth, perhaps with a dominance of thermogenic methane. However, while elevated values for the walking transects were observed in close proximity to the pingo features, we note that for both sites the highest values were not on the features themselves, but a short distance away in the low lying shrub tundra terrain surrounding the pingos.

Most pingos in the Tuktoyaktuk Peninsula area generally form in areas of thick permafrost with drained lacustrine basins and are therefore assumed to be closed system pingos formed from re-freezing of a local talik beneath the drained lakes. However, because permafrost is thin in the outer MRD, the pingos in this area can be open system pingos formed from fluid migration from beneath the permafrost interval (Mackay, 1963). We conclude that the Pingo 1 and 2 features are most likely open system pingos as they have formed in a flat lying delta plain setting with no indication of a drained lake and nearby scientific drilling indicates only about 80 m of thermally defined permafrost and perhaps only 50-60 m of ice bonded permafrost (Dallimore et al., 1992). While formed in a different geologic setting, Hodson et al. (2019) have found methane occurrences in groundwater discharges in the vicinity of open system pingos in Svalbard. In this case, the isotope signature of  $\text{CH}_4$  in groundwater was similar to that found below the permafrost. We note a similar relationship for the pingo sites in the outer delta where scientific drilling conducted at the Unipkat well site found an isotopic  $\delta^{13}\text{C}-\text{CH}_4$  value of -53‰ dissolved methane in core samples beneath the ice bonded permafrost interval (Collett and Dallimore, 1999). This is an identical value to Keeling plot determinations for the Pingo 1 site and similar to that found at Pingo 2. A point of interest, however, is that the methane concentrations over the pingo features themselves were only as high 2.2 ppm with the highest values in the walking transect 200-400 m distant from the pingo. One possibility for this occurrence is that the signal from the pingo itself may have been shifted by wind, however measured wind velocity and direction during the survey did not seem consistent with this possibility. Given that the ice bonded permafrost in the pingo itself is likely impermeable to fluid and gas flux, we conclude that the local source is likely from the terrain surrounding the pingo where indeed open system ground water flow may be occurring. Further research including repeat ground sampling transects and possible permafrost geophysics is warranted to constrain this hypothesis.

Collapsed Pingo 3 was formed in a much different environment than Pingo 1 and 2, in the Tuktoyaktuk coastal plain where the permafrost is > 500 m thick (Todd and Dallimore, 1998). Migration of  $\text{CH}_4$  through the permafrost is much less likely here than in the outer MRD. In this case, gas release was as ebullition through a small pond with a Keeling plot stable carbon isotope source signature of -73.6 ‰ suggesting a more definitive biogenic methane source. As the permafrost is much thicker at this site, the potential for a talik penetrating the entire permafrost and providing a conduit for migration of deep thermogenic methane is much less likely.

Hodson et al. (2020) found that six pingos in Svalbard had a range of annual flux rates between 76.4 and 364 kg  $\text{CH}_4$ /year and concluded that pingos require further study due to their potential contributions of  $\text{CH}_4$  to the atmosphere. The





outer MRD and the Pleistocene deposits of the Tuktoyaktuk Peninsula are home to about 2363 pingos (Wolfe et al., 2021). Release of CH<sub>4</sub> from pingos in the region could represent a significant, unaccounted source of CH<sub>4</sub> to the atmosphere making it a critical area for further study of pingos as a source of CH<sub>4</sub>. Migration of CH<sub>4</sub> to the atmosphere from pingos is still poorly understood and additional studies of CH<sub>4</sub> production from pingos will help to improve Arctic CH<sub>4</sub> emission estimates.

## 260 **Wetland sites**

Three wetland sites were co-located with airborne eddy covariance identified hotspot sites that occurred in rather flat delta plain settings in the western part of the outer MRD (Figure 1). These sites had no obvious geologic or permafrost features or local ebullition sites in water bodies. They were dominated by low shrub tundra with some areas of exposed delta sediments with sparse sedges. We characterized these as wetlands as much of the surface had 10-30 cm of standing water. No elevated atmospheric methane values were detected during walking transects at Site 9, however concentrations of 2.152 ppm were observed at Wetland 2 and 2.264 ppm at Wetland 3. At both sites modestly elevated values above background were found along most of the walking transects. Estimates of source stable carbon isotope signatures ( $\delta^{13}\text{C-CH}_4$ ) derived from Keeling plots were -78.4‰ for Wetland 2 and -71.9‰ for Wetland 3. Elevated CO<sub>2</sub> values up to 603 ppm were observed at Wetland 2. The lack of a methane signal at Site 9 and the low values at Wetland 2 and 3 do not provide substantive validation of a possible source for the eddy covariance hotspots observed by Kohnert et al. (2017). However, it is reasonable to consider that these featureless delta plain areas of the MRD may be dominated by widely dispersed methane flux from mainly biogenic sources. Elevated CO<sub>2</sub> of 603 ppm at Wetland 2 may also support this inference since co-generation of CH<sub>4</sub> with CO<sub>2</sub> is typical of biogenic production.

Discrete sampling at Wetland 1 yielded  $\delta^{13}\text{C-CH}_4$  Keeling plot source signature of -88.3‰ when sampled in October during freeze up and -53.4‰ during the summer. In simple terms, this suggests a biogenic source when sampled in October but a mixed source when sampled during the summer. While the sampling was carried out at the same location, methane ebullition was seen while sampling during the fall, but not during the summer. The Wetland 1 site was dominated by sedge vegetation with areas of standing water. We conclude that this demonstrates a biogenic source during the fall since biogenic production can persist late into the cold season (Zona et al., 2016). The lack of ebullition flux at the same site during the summer and the different Keeling plot estimate suggest methane flux in this wetland setting varies seasonally. The Keeling plot source signature of -53.4‰ during the summer could be caused from either oxidation of a biogenic source or contributions of both biogenic and thermogenic sources. Seasonal shifts in lake-produced CH<sub>4</sub> stable carbon isotope signatures potentially due to oxidation are known to occur but are typically observed during winter beneath ice cover (Michmerhuizen et al., 1996; Ettwig et al., 2016), or the transition from the ice covered to open water periods in the spring (McIntosh Marcek et al., 2021). Similar observations for seasonal variability in terrestrial sources are not well documented in the literature, although transport of CH<sub>4</sub> from anaerobic soils with sedge vegetation has been observed to bypass the aerobic zone, limiting oxidation during the growing season (Olefeldt et al., 2013; King et al., 1998). Therefore, it is possible that there were contributions to the atmosphere



from biogenic and thermogenic sources at Wetland 1, but oxidation and varying production pathways cannot be ruled out as the reason for the signature derived during the summer sampling.

## 290 **5.2 Methane from ebullition sources in the MRD and Tuktoyaktuk Coastlands**

Some of the largest occurrences of atmospheric release of CH<sub>4</sub> in Arctic environments have been reported in association with large gas seeps of thermogenic CH<sub>4</sub>, causing high-rate ebullition (Walter Anthony et al., 2012). The Channel Seep sampled in this study was at the edge of a small river channel with high-rate ebullition observed during our field work. This site had a δ<sup>13</sup>C-CH<sub>4</sub> Keeling plot source signature of -42.0 ‰. Lake 1 which was conducted in the immediate vicinity of a smaller ebullition stream also had a very similar source signature of -44.7 ‰. When combined with sampling of a vigorous ebullition in a small pond by Bowen et al. (2008) with -43.3 ‰ values, three locations with similar ebullition character and isotopic values are spaced over approximately 20 km in a north-south trend. We note that the Niglingtak/Kumak hydrocarbon field, which occurs only 5 km to the east of these sites, occurs in a faulted anticline structure with the same trend. While no data is available for this field, thermogenic gas observed at the nearby Taglu field with similar geology varied from -25 to -50 ‰ for multiple gas horizons at depths from 1700 to > 4000 m depth (Collett and Dallimore, 1999). As the permafrost is less than 80 m thick in this area, it is probable that the high ebullition sites occur where taliks have formed through the permafrost creating a migration pathway for thermogenic gasses to pass through the permafrost. In addition, a common thermogenic signature at multiple sites in close proximity but different settings suggests a possible pervasive regional source.

Flux chamber sampling over the terrestrial shrub tundra terrain immediately adjacent to Lake 1 indicated it was a source of CH<sub>4</sub> and CO<sub>2</sub> with flux rates of 2.25 mg CH<sub>4</sub>-C hr<sup>-1</sup>m<sup>-2</sup> and 52.73 mg CO<sub>2</sub>-C hr<sup>-1</sup>m<sup>-2</sup>. The soil adjacent to Lake 1 was saturated with water creating ideal conditions for biogenic production at the site. This shows that we sampled multiple sources of CH<sub>4</sub> at the site; biogenic methane production in and around the lake as well as a strong thermogenic seep. This could account for the low r<sup>2</sup> value (0.48) (Fig. 3) at Lake 1 despite highly elevated CH<sub>4</sub>.

## **6 Conclusion**

To our knowledge, this is the first study to measure stable carbon isotope signatures of atmospheric methane at hotspots in the MRD. Estimates of source isotope signatures from field sites varied substantially from biogenic to thermogenic, indicating that the largest sites of CH<sub>4</sub> production in the MRD are caused by a variety of sources. Of eight sites investigated in this study, two were thermogenic in origin, four were biogenic in origin, and two were from mixed biogenic/thermogenic sources, as evidenced by stable carbon isotope signatures and the high potential for migration of CH<sub>4</sub> from below the thin permafrost at the majority of these sites. In addition to biogenic production at the surface, we have identified CH<sub>4</sub> migration to the surface from the Taglu gas field over an area of approximately 20 km from north to south and two different sites of mixed biogenic/thermogenic CH<sub>4</sub> that were approximately 30 km apart.



In this study we were able to verify airborne eddy covariance hotspot locations using walking transects to measure atmospheric variation of CH<sub>4</sub>. These methods can still be improved as they only provide a snapshot of methane sources to the atmosphere during site visits and a true picture of annual CH<sub>4</sub> production cannot be established here. Future research should include year-round flux measurements at these sites, coupled with stable carbon isotope measurements. This would fully quantify the annual CH<sub>4</sub> emission to the atmosphere from biogenic and thermogenic sources at these sites. This study attempted to verify CH<sub>4</sub> hotspots identified from airborne eddy covariance surveys and determine their source at the same time. Because sites from remote sensing surveys were large and areal in nature, verification required covering large areas by foot. Not only is this time consuming but can make it difficult to pinpoint exact emission locations. Combined use of portable CH<sub>4</sub> analysers with flux chamber and isotopic measurements at the locations of the highest atmospheric mixing ratios of CH<sub>4</sub> would be a more direct and methodical way separate and quantify sources, especially at sites where both biogenic and thermogenic sources are likely.

### Competing Interests

The authors declare that there are no competing interests

### Author Contribution

DW conceptualization, investigation, formal analysis, original draft preparation, reviewing and editing. SD funding acquisition, conceptualization, reviewing and editing. RM investigation, reviewing and editing. TS reviewing and editing. DR funding acquisition, conceptualization, reviewing and editing. All of the authors edited and approved the final version for submission.

### Acknowledgements

We would like to acknowledge the following contributions to this work. The LiCor gas analyser used for sampling was kindly provided by Jacqueline Goordial. Support during fieldwork was provided by Jacqueline Goordial, Peter Morse and Isaac Ketchum. Samples from Lake 1 were collected by Julia Boike. Some sample analysis was provided by Laura Lapham. Fieldwork costs were supplemented by the Northern Scientific Training Program.



## References

- 345 Allan, W., Manning, M. R., Lassey, K. R., Lowe, D. C., and Gomez, A. J.: Modeling the variation of  $\delta^{13}\text{C}$  in atmospheric methane: Phase ellipses and the kinetic isotope effect, *Glob. Biogeochem. Cycles*, 15, 467–481, <https://doi.org/10.1029/2000GB001282>, 2001.
- Andersen, T., Scheeren, B., Peters, W., and Chen, H.: A UAV-based active AirCore system for measurements of greenhouse gases, *Atmospheric Meas. Tech.*, 11, 2683–2699, <https://doi.org/10.5194/amt-11-2683-2018>, 2018.
- 350 Biskaborn, B. K., Smith, S. L., Noetzli, J., Matthes, H., Vieira, G., Streletskiy, D. A., Schoeneich, P., Romanovsky, V. E., Lewkowicz, A. G., Abramov, A., Allard, M., Boike, J., Cable, W. L., Christiansen, H. H., Delaloye, R., Diekmann, B., Drozdov, D., Etzelmüller, B., Grosse, G., Guglielmin, M., Ingeman-Nielsen, T., Isaksen, K., Ishikawa, M., Johannsson, M., Johannsson, H., Joo, A., Kaverin, D., Kholodov, A., Konstantinov, P., Kröger, T., Lambiel, C., Lanckman, J.-P., Luo, D., Malkova, G., Meiklejohn, I., Moskalenko, N., Oliva, M., Phillips, M., Ramos, M., Sannel, A. B. K., Sergeev, D., Seybold, C., Skryabin, P., Vasiliev, A., Wu, Q., Yoshikawa, K., Zheleznyak, M., and Lantuit, H.: Permafrost is warming at a global scale, *Nat. Commun.*, 10, 264, <https://doi.org/10.1038/s41467-018-08240-4>, 2019.
- 355 Bowen, R. G., Dallimore, S. R., Côté, M. M., Wright, J. F., and Lorenson, T. D.: Geomorphology and gas release from pockmark features in the Mackenzie Delta, Northwest Territories, Canada., 6, 2008.
- Brownlow, R., Lowry, D., Fisher, R. E., France, J. L., Lanoisellé, M., White, B., Wooster, M. J., Zhang, T., and Nisbet, E. G.: Isotopic Ratios of Tropical Methane Emissions by Atmospheric Measurement: Tropical Methane  $\delta^{13}\text{C}$  Source Signatures, *Glob. Biogeochem. Cycles*, 31, 1408–1419, <https://doi.org/10.1002/2017GB005689>, 2017.
- 360 Burn, C. R.: Tundra lakes and permafrost, Richards Island, western Arctic coast, Canada., *Can. J. Earth Sci.*, 39, 1281–1298, 2002.
- Burn, C. R.: Lake-bottom thermal regimes, western Arctic coast, Canada, *Permafr. Periglac. Process.*, 16, 355–367, <https://doi.org/10.1002/ppp.542>, 2005.
- 365 Burn, C. R. and Kokelj, S. V.: The environment and permafrost of the Mackenzie Delta area, *Permafr. Periglac. Process.*, 20, 83–105, <https://doi.org/10.1002/ppp.655>, 2009.
- Collett, T. S. and Dallimore, S. R.: Hydrocarbon gases associated with permafrost in the Mackenzie Delta, Northwest Territories, Canada, *Appl. Geochem.*, 14, 607–620, [https://doi.org/10.1016/S0883-2927\(98\)00087-0](https://doi.org/10.1016/S0883-2927(98)00087-0), 1999.
- 370 Collins, M., Knutti, R., Arblaster, J., Dufresne, J.-L., Fichefet, T., Gao, X., Jr, W. J. G., Johns, T., Krinner, G., Shongwe, M., Weaver, A. J., Wehner, M., Allen, M. R., Andrews, T., Beyerle, U., Bitz, C. M., Bony, S., Booth, B. B. B., Brooks, H. E., Brovkin, V., Browne, O., Brutel-Vuilmet, C., Cane, M., Chadwick, R., Cook, E., Cook, K. H., Eby, M., Fasullo, J., Forest, C. E., Forster, P., Good, P., Goosse, H., Gregory, J. M., Hegerl, G. C., Hezel, P. J., Hodges, K. I., Holland, M. M., Huber, M., Joshi, M., Kharin, V., Kushnir, Y., Lawrence, D. M., Lee, R. W., Liddicoat, S., Lucas, C., Lucht, W., Marotzke, J., Massonnet, F., Matthews, H. D., Meinshausen, M., Morice, C., Otto, A., Patricola, C. M., Philippon, G., Rahmstorf, S., Riley, W. J., Saenko, O., Seager, R., Sedláček, J., Shaffrey, L. C., Shindell, D., Sillmann, J., Stevens, B., Stott, P. A., Webb, R., Zappa, G.,
- 375 Zickfeld, K., Joussaume, S., Mokssit, A., Taylor, K., and Tett, S.: Long-term Climate Change: Projections, Commitments and Irreversibility, in: *Climate Change 2013: The Physical Science Basis. Contribution of Working Group I to the Fifth Assessment Report of the Intergovernmental Panel on Climate Change*, Cambridge University Press, Cambridge, UK, 108, 2013.
- Dallimore, S. R., Allen, V. S., Blondheim, F., Bisson, J. G., Carron, J., Davies, E., Davidson, K., and Dixon, J.: *Borehole Logs From Joint GSC - Industry Mackenzie Delta Geology / Permafrost Transect*, Geological Survey of Canada, 1992.



- 380 Dean, J. F., Middelburg, J. J., Röckmann, T., Aerts, R., Blauw, L. G., Egger, M., Jetten, M. S. M., de Jong, A. E. E., Meisel, O. H., Rasigraf, O., Slomp, C. P., in't Zandt, M. H., and Dolman, A. J.: Methane Feedbacks to the Global Climate System in a Warmer World, *Rev. Geophys.*, 56, 207–250, <https://doi.org/10.1002/2017RG000559>, 2018.
- Ecosystem Classification Group: Ecological regions of the Northwest Territories: Taiga Plains, Dept. of Environment and Natural Resources, Govt. of the Northwest Territories, Yellowknife, NWT, 2009.
- 385 Ecosystem Classification Group: Ecological regions of the Northwest Territories, southern Arctic, Dept. of Environment and Natural Resources, Govt. of the Northwest Territories, Yellowknife, 2012.
- Emmerton, C. A., Lesack, L. F. W., and Marsh, P.: Lake abundance, potential water storage, and habitat distribution in the Mackenzie River Delta, western Canadian Arctic, 14, 2007.
- Ettwig, K. F., Zhu, B., Speth, D., Keltjens, J. T., Jetten, M. S. M., and Kartal, B.: Archaea catalyze iron-dependent anaerobic oxidation of methane, *Proc. Natl. Acad. Sci.*, 113, 12792–12796, <https://doi.org/10.1073/pnas.1609534113>, 2016.
- 390 Farquharson, L. M., Romanovsky, V. E., Cable, W. L., Walker, D. A., Kokelj, S. V., and Nicolsky, D.: Climate Change Drives Widespread and Rapid Thermokarst Development in Very Cold Permafrost in the Canadian High Arctic, *Geophys. Res. Lett.*, 46, 6681–6689, <https://doi.org/10.1029/2019GL082187>, 2019.
- Friborg, T., Christensen, T. R., Hansen, B. U., Nordstroem, C., and Soegaard, H.: Trace gas exchange in a high-Arctic valley: 2. Landscape CH<sub>4</sub> fluxes measured and modeled using eddy correlation data, *Glob. Biogeochem. Cycles*, 14, 715–723, <https://doi.org/10.1029/1999GB001136>, 2000.
- 395 Gill, D.: The Point Bar Environment in the Mackenzie River Delta, *Can. J. Earth Sci.*, 9, 1382–1393, <https://doi.org/10.1139/e72-125>, 1972.
- GRID-Arendal: Coastal and Offshore Permafrost in a Changing Arctic. In: Rapid Response Assessment of Coastal and Offshore Permafrost, Story Map, 2020.
- 400 Hill, P. R., Lewis, C. P., Desmarais, S., Kauppaymuthoo, V., and Rais, H.: The Mackenzie Delta: sedimentary processes and facies of a high-latitude, fine-grained delta, *Sedimentology*, 48, 1047–1078, <https://doi.org/10.1046/j.1365-3091.2001.00408.x>, 2001.
- Hodson, A. J., Nowak, A., Redeker, K. R., Holmlund, E. S., Christiansen, H. H., and Turchyn, A. V.: Seasonal Dynamics of Methane and Carbon Dioxide Evasion From an Open System Pingo: Lagoon Pingo, Svalbard, *Front. Earth Sci.*, 7, 30, <https://doi.org/10.3389/feart.2019.00030>, 2019.
- 405 Hodson, A. J., Nowak, A., Senger, K., Redeker, K., Christiansen, H. H., Jessen, S., Hornum, M. T., Betlem, P., Thornton, S. F., Turchyn, A. V., Olausson, S., and Marca, A.: Open system pingos as hotspots for sub-permafrost methane emission in Svalbard, *The Cryosphere*, <https://doi.org/10.5194/tc-2020-11>, 2020.
- 410 Keeling, C. D.: The concentration and isotopic abundances of atmospheric carbon dioxide in rural areas, *Geochim. Cosmochim. Acta*, 13, 322–334, [https://doi.org/10.1016/0016-7037\(58\)90033-4](https://doi.org/10.1016/0016-7037(58)90033-4), 1958.
- Keeling, C. D.: The concentration and isotopic abundances of carbon dioxide in rural and marine air, *Geochim. Cosmochim. Acta*, 24, 277–298, [https://doi.org/10.1016/0016-7037\(61\)90023-0](https://doi.org/10.1016/0016-7037(61)90023-0), 1961.
- 415 King, J. Y., Reeburgh, W. S., and Regli, S. K.: Methane emission and transport by arctic sedges in Alaska: Results of a vegetation removal experiment, *J. Geophys. Res. Atmospheres*, 103, 29083–29092, <https://doi.org/10.1029/98JD00052>, 1998.



- 420 Kirschke, S., Bousquet, P., Ciais, P., Saunoy, M., Canadell, J. G., Dlugokencky, E. J., Bergamaschi, P., Bergmann, D., Blake, D. R., Bruhwiler, L., Cameron-Smith, P., Castaldi, S., Chevallier, F., Feng, L., Fraser, A., Heimann, M., Hodson, E. L., Houweling, S., Josse, B., Fraser, P. J., Krummel, P. B., Lamarque, J.-F., Langenfelds, R. L., Le Quéré, C., Naik, V., O'Doherty, S., Palmer, P. I., Pison, I., Plummer, D., Poulter, B., Prinn, R. G., Rigby, M., Ringeval, B., Santini, M., Schmidt, M., Shindell, D. T., Simpson, I. J., Spahni, R., Steele, L. P., Strode, S. A., Sudo, K., Szopa, S., van der Werf, G. R., Voulgarakis, A., van Weele, M., Weiss, R. F., Williams, J. E., and Zeng, G.: Three decades of global methane sources and sinks, *Nat. Geosci.*, 6, 813–823, <https://doi.org/10.1038/ngeo1955>, 2013.
- Kohler, P., Fischer, H., Schmitt, J., and Munhoven, G.: On the application and interpretation of Keeling plots in paleo climate research – deciphering  $\delta^{13}\text{C}$  of atmospheric  $\text{CO}_2$  measured in ice cores, 18, 2006.
- 425 Kohnert, K., Serafimovich, A., Metzger, S., Hartmann, J., and Sachs, T.: Strong geologic methane emissions from discontinuous terrestrial permafrost in the Mackenzie Delta, Canada, *Sci. Rep.*, 7, 5828, <https://doi.org/10.1038/s41598-017-05783-2>, 2017.
- Kohnert, K., Juhls, B., Muster, S., Antonova, S., Serafimovich, A., Metzger, S., Hartmann, J., and Sachs, T.: Toward understanding the contribution of waterbodies to the methane emissions of a permafrost landscape on a regional scale-A case study from the Mackenzie Delta, Canada, *Glob. Change Biol.*, 24, 3976–3989, <https://doi.org/10.1111/gcb.14289>, 2018.
- 430 Lewis, C. P.: Mackenzie Delta sedimentary environments and processes, Unpubl. Contract Rep. Environ. Can. Sediment Surv. Ott. Ont., 1988.
- Mackay, J. R.: The Mackenzie Delta Area, N.W.T., 212, 1963.
- Mamet, S. D., Chun, K. P., Kershaw, G. G. L., Lorant, M. M., and Peter Kershaw, G.: Recent Increases in Permafrost Thaw Rates and Areal Loss of Palsas in the Western Northwest Territories, Canada: Non-linear Palsa Degradation, *Permafrost Process.*, 28, 619–633, <https://doi.org/10.1002/ppp.1951>, 2017.
- 435 Marsh, P.: Permafrost and lakes in the Mackenzie Delta, *Proc. Fifth Can. Permafrost Conf.*, 54, 1990.
- McIntosh Marcek, H. A., Lesack, L. F. W., Orcutt, B. N., Wheat, C. G., Dallimore, S. R., Geeves, K., and Lapham, L. L.: Continuous Dynamics of Dissolved Methane Over 2 Years and its Carbon Isotopes ( $\delta^{13}\text{C}$ ,  $\Delta^{14}\text{C}$ ) in a Small Arctic Lake in the Mackenzie Delta, *J. Geophys. Res. Biogeosciences*, 126, <https://doi.org/10.1029/2020JG006038>, 2021.
- 440 Michmerhuizen, C. M., Striegl, R. G., and McDonald, M. E.: Potential methane emission from north-temperate lakes following ice melt, *Limnol. Oceanogr.*, 41, 985–991, <https://doi.org/10.4319/lo.1996.41.5.0985>, 1996.
- Nguyen, T.-N., Burn, C. R., King, D. J., and Smith, S. L.: Estimating the extent of near-surface permafrost using remote sensing, Mackenzie Delta, Northwest Territories, *Permafrost Periglac. Process.*, 20, 141–153, <https://doi.org/10.1002/ppp.637>, 2009.
- 445 Nisbet, E. G., Dlugokencky, E. J., Manning, M. R., Lowry, D., Fisher, R. E., France, J. L., Michel, S. E., Miller, J. B., White, J. W. C., Vaughn, B., Bousquet, P., Pyle, J. A., Warwick, N. J., Cain, M., Brownlow, R., Zazzeri, G., Lanouisellé, M., Manning, A. C., Gloor, E., Worthy, D. E. J., Brunke, E.-G., Labuschagne, C., Wolff, E. W., and Ganesan, A. L.: Rising atmospheric methane: 2007–2014 growth and isotopic shift: RISING METHANE 2007–2014, *Glob. Biogeochem. Cycles*, 30, 1356–1370, <https://doi.org/10.1002/2016GB005406>, 2016.
- Olefeldt, D., Turetsky, M. R., Crill, P. M., and McGuire, A. D.: Environmental and physical controls on northern terrestrial methane emissions across permafrost zones, *Glob. Change Biol.*, 19, 589–603, <https://doi.org/10.1111/gcb.12071>, 2013.

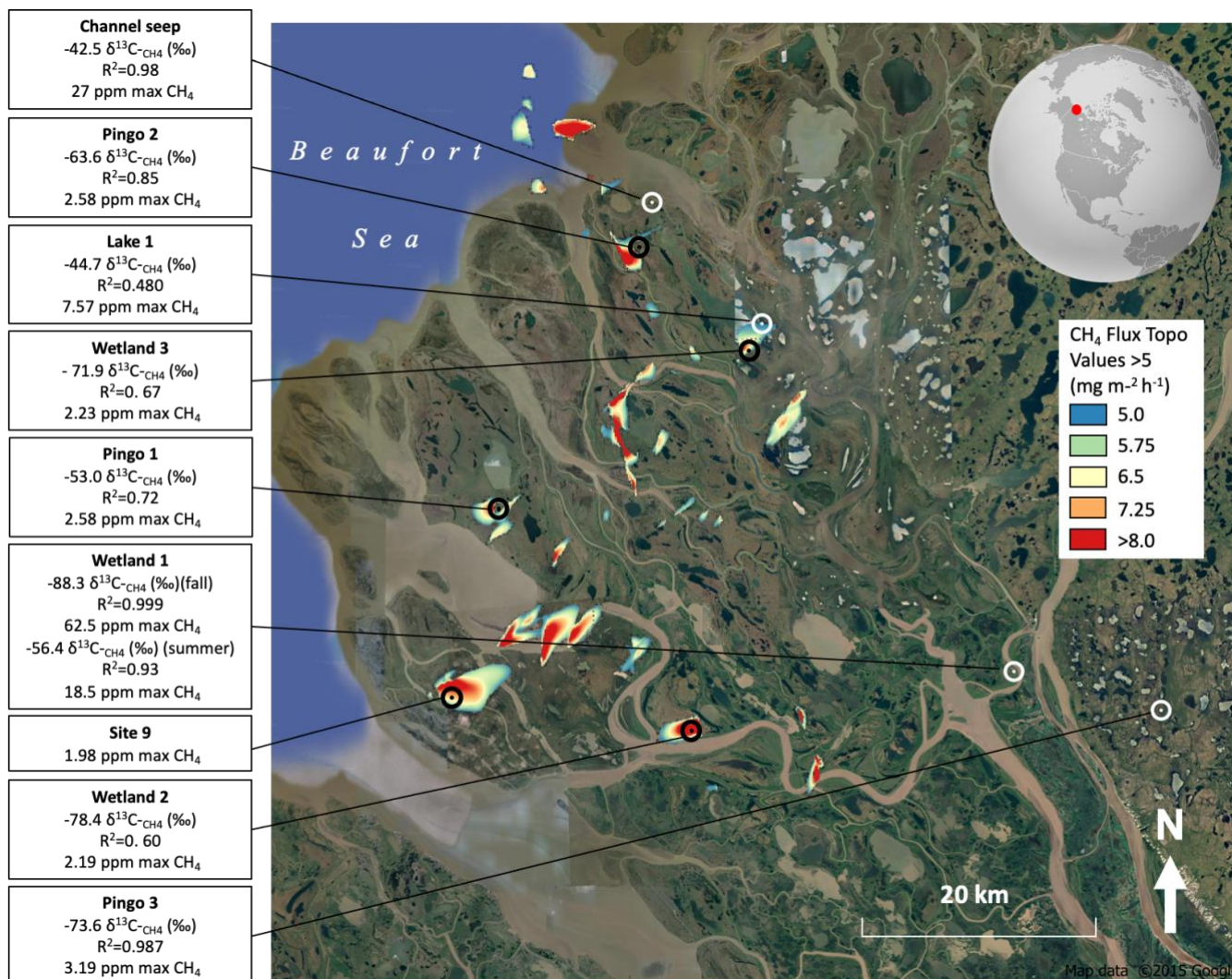




- 455 Osadetz, K. G. and Chen, Z.: A re-evaluation of Beaufort Sea-Mackenzie Delta basin gas hydrate resource potential: petroleum system approaches to non-conventional gas resource appraisal and geologically-sourced methane flux, *Bull. Can. Pet. Geol.*, 58, 56–71, <https://doi.org/10.2113/gscpgbull.58.1.56>, 2010.
- Pataki, D. E., Ehleringer, J. R., Flanagan, L. B., Yakir, D., Bowling, D. R., Still, C. J., Buchmann, N., Kaplan, J. O., and Berry, J. A.: The application and interpretation of Keeling plots in terrestrial carbon cycle research: APPLICATION OF KEELING PLOTS, *Glob. Biogeochem. Cycles*, 17, <https://doi.org/10.1029/2001GB001850>, 2003.
- 460 Rawlins, M. A., Steele, M., Holland, M. M., Adam, J. C., Cherry, J. E., Francis, J. A., Groisman, P. Y., Hinzman, L. D., Huntington, T. G., Kane, D. L., Kimball, J. S., Kwok, R., Lammers, R. B., Lee, C. M., Lettenmaier, D. P., McDonald, K. C., Podest, E., Pundsack, J. W., Rudels, B., Serreze, M. C., Shiklomanov, A., Skagseth, Ø., Troy, T. J., Vörösmarty, C. J., Wensnahan, M., Wood, E. F., Woodgate, R., Yang, D., Zhang, K., and Zhang, T.: Analysis of the Arctic System for Freshwater Cycle Intensification: Observations and Expectations, *J. Clim.*, 23, 5715–5737, <https://doi.org/10.1175/2010JCLI3421.1>, 2010.
- 465 Sachs, T., Wille, C., Boike, J., and Kutzbach, L.: Environmental controls on ecosystem-scale CH<sub>4</sub> emission from polygonal tundra in the Lena River Delta, Siberia, *J. Geophys. Res.*, 113, G00A03, <https://doi.org/10.1029/2007JG000505>, 2008.
- Saunio, M., Bousquet, P., Poulter, B., Peregón, A., Ciais, P., Canadell, J. G., Dlugokencky, E. J., Etiope, G., Bastviken, D., Houweling, S., Janssens-Maenhout, G., Tubiello, F. N., Castaldi, S., Jackson, R. B., Alexe, M., Arora, V. K., Beerling, D. J., Bergamaschi, P., Blake, D. R., Brailsford, G., Brovkin, V., Bruhwiler, L., Crevoisier, C., Crill, P., Covey, K., Curry, C., 470 Frankenberg, C., Gedney, N., Höglund-Isaksson, L., Ishizawa, M., Ito, A., Joos, F., Kim, H.-S., Kleinen, T., Krummel, P., Lamarque, J.-F., Langenfelds, R., Locatelli, R., Machida, T., Maksyutov, S., McDonald, K. C., Marshall, J., Melton, J. R., Morino, I., Naik, V., O’Doherty, S., Parmentier, F.-J. W., Patra, P. K., Peng, C., Peng, S., Peters, G. P., Pison, I., Prigent, C., Prinn, R., Ramonet, M., Riley, W. J., Saito, M., Santini, M., Schroeder, R., Simpson, I. J., Spahni, R., Steele, P., Takizawa, A., Thornton, B. F., Tian, H., Tohjima, Y., Viovy, N., Voulgarakis, A., van Weele, M., van der Werf, G. R., Weiss, R., 475 Wiedinmyer, C., Wilton, D. J., Wiltshire, A., Worthy, D., Wunch, D., Xu, X., Yoshida, Y., Zhang, B., Zhang, Z., and Zhu, Q.: The global methane budget 2000–2012, *Earth Syst. Sci. Data*, 8, 697–751, <https://doi.org/10.5194/essd-8-697-2016>, 2016.
- Schoell, M.: The hydrogen and carbon isotopic composition of methane from natural gases of various origins, *Geochim. Cosmochim. Acta*, 44, 649–661, [https://doi.org/10.1016/0016-7037\(80\)90155-6](https://doi.org/10.1016/0016-7037(80)90155-6), 1980.
- 480 Schuur, E. A. G., Bockheim, J., Canadell, J. G., Euskirchen, E., Field, C. B., Goryachkin, S. V., Hagemann, S., Kuhry, P., Lafleur, P. M., Lee, H., Mazhitova, G., Nelson, F. E., Rinke, A., Romanovsky, V. E., Shiklomanov, N., Tarnocai, C., Venevsky, S., Vogel, J. G., and Zimov, S. A.: Vulnerability of Permafrost Carbon to Climate Change: Implications for the Global Carbon Cycle, *BioScience*, 58, 701–714, <https://doi.org/10.1641/B580807>, 2008.
- Sturtevant, C. S., Oechel, W. C., Zona, D., Kim, Y., and Emerson, C. E.: Soil moisture control over autumn season methane flux, Arctic Coastal Plain of Alaska, *Biogeosciences*, 9, 1423–1440, <https://doi.org/10.5194/bg-9-1423-2012>, 2012.
- 485 Todd, B. J. and Dallimore, S. R.: Electromagnetic and geological transect across permafrost terrain, Mackenzie River delta, Canada, *GEOPHYSICS*, 63, 1914–1924, <https://doi.org/10.1190/1.1444484>, 1998.
- Treat, C. C., Marushchak, M. E., Voigt, C., Zhang, Y., Tan, Z., Zhuang, Q., Virtanen, T. A., Räsänen, A., Biasi, C., Hugelius, G., Kaverin, D., Miller, P. A., Stendel, M., Romanovsky, V., Rivkin, F., Martikainen, P. J., and Shurpali, N. J.: Tundra landscape heterogeneity, not interannual variability, controls the decadal regional carbon balance in the Western Russian 490 Arctic, *Glob. Change Biol.*, 24, 5188–5204, <https://doi.org/10.1111/gcb.14421>, 2018.
- Walker, H. J.: Arctic Deltas, *J. Coast. Res.*, 14, 22, 1998.



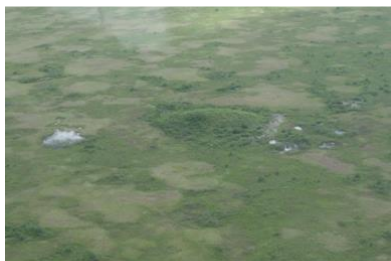
- Walter Anthony, K. M., Vas, Dragos. A., Brosius, L., Chapin, F. S., Zimov, S. A., and Zhuang, Q.: Estimating methane emissions from northern lakes using ice-bubble surveys: Methane bubbles in lake ice method, *Limnol. Oceanogr. Methods*, 8, 592–609, <https://doi.org/10.4319/lom.2010.8.0592>, 2010.
- 495 Walter Anthony, K. M., Anthony, P., Grosse, G., and Chanton, J.: Geologic methane seeps along boundaries of Arctic permafrost thaw and melting glaciers, *Nat. Geosci.*, 5, 419–426, <https://doi.org/10.1038/ngeo1480>, 2012.
- Walter, K. M., Zimov, S. A., Chanton, J. P., Verbyla, D., and Chapin, F. S.: Methane bubbling from Siberian thaw lakes as a positive feedback to climate warming, *Nature*, 443, 71–75, <https://doi.org/10.1038/nature05040>, 2006.
- 500 Wik, M., Varner, R. K., Anthony, K. W., MacIntyre, S., and Bastviken, D.: Climate-sensitive northern lakes and ponds are critical components of methane release, *Nat. Geosci.*, 9, 99–105, <https://doi.org/10.1038/ngeo2578>, 2016.
- Wolfe, S. A., Morse, P. D., and Behnia, P.: Spatial distribution of pingos in the Tuktoyaktuk coastlands and adjacent areas, Northwest Territories, <https://doi.org/10.4095/328305>, 2021.
- Zona, D., Gioli, B., Commane, R., Lindaas, J., Wofsy, S. C., Miller, C. E., Dinardo, S. J., Dengel, S., Sweeney, C., Karion, A., Chang, R. Y.-W., Henderson, J. M., Murphy, P. C., Goodrich, J. P., Moreaux, V., Liljedahl, A., Watts, J. D., Kimball, J. S., Lipson, D. A., and Oechel, W. C.: Cold season emissions dominate the Arctic tundra methane budget, *Proc. Natl. Acad. Sci.*, 113, 40–45, <https://doi.org/10.1073/pnas.1516017113>, 2016.



510 **Figure 1: Methane stable carbon isotope source signatures at sample sites in the Mackenzie River Delta. Locations are superimposed**  
**on a map of  $\text{CH}_4$  flux rates published by Kohnert et al. (2017) Signatures varied from -42 to -88 ‰  $\delta^{13}\text{C-CH}_4$  indicating that the**  
**source of  $\text{CH}_4$  varied at different sites and ranged from entirely thermogenic (indicated by less negative ‰ values) to entirely biogenic**  
**to a mixture of both biogenic and thermogenic. Source signatures were derived from regression of keeling plots which were based**  
**on point samples of atmospheric methane. Black symbols indicate sites identified by Kohnert et al. (2017). White symbols indicate**  
 515 **sites identified by  $\text{CH}_4$  ebullition.**

520





Pingo 1: A large (> 1 km wide) CH<sub>4</sub> hotspot identified by Kohnert et al. (2017). The pingo itself was approximately 95 m wide and 7.5 m high. Discrete point samples and walking transects were taken around the pingo in the area where the highest flux rates were observed by Kohnert et al. (2017).



Pingo 2: A large (> 1 km wide) CH<sub>4</sub> hotspot identified by Kohnert et al. (2017). The pingo was approximately 60 m wide and 6 m high with wetlands and a large lake to the southwest. The pingo was located on the very edge of the hotspot but near where the highest flux rate was observed by Kohnert et al. (2017). Discrete point samples and walking transects were taken around the pingo and to the southwest of the pingo near the wetland.



Pingo 3: A collapsed Pingo of about 80 m in diameter with a lake formed in the resulting crater. Discrete point samples were taken during the fall, close to holes in the ice and outside of the crater. Discrete point samples and walking transects were taken around the edge and outside of the crater during an additional summer field campaign. Flux chamber measurements were taken at the outlet of the lake in a sedge covered area.



Wetland 1: A sedge dominated wetland of about 80 m in diameter. Discrete point samples were taken near holes in the ice and along the edge of the lake during the fall. Discrete point samples and walking transect were taken during an additional summer field campaign in the same location as the fall samples.



Wetland 2: A broad CH<sub>4</sub> hotspot (~ 800 m wide) identified by Kohnert et al. (2017). The site was comprised of tussock tundra dotted by many small wetlands and a few shrubs. Field of view is approximately 10 m wide. Discrete point samples and walking transects were taken where the highest flux rates were observed by Kohnert et al. (2017).



Wetland 3: A broad (~ 600 m wide) CH<sub>4</sub> hotspot identified by Kohnert et al. (2017) with mixture of wetland and grassland with patches of alders. Field of view is approximately 40 m wide. Samples and walking transects were taken where the highest flux rate was observed by Kohnert et al. (2017).

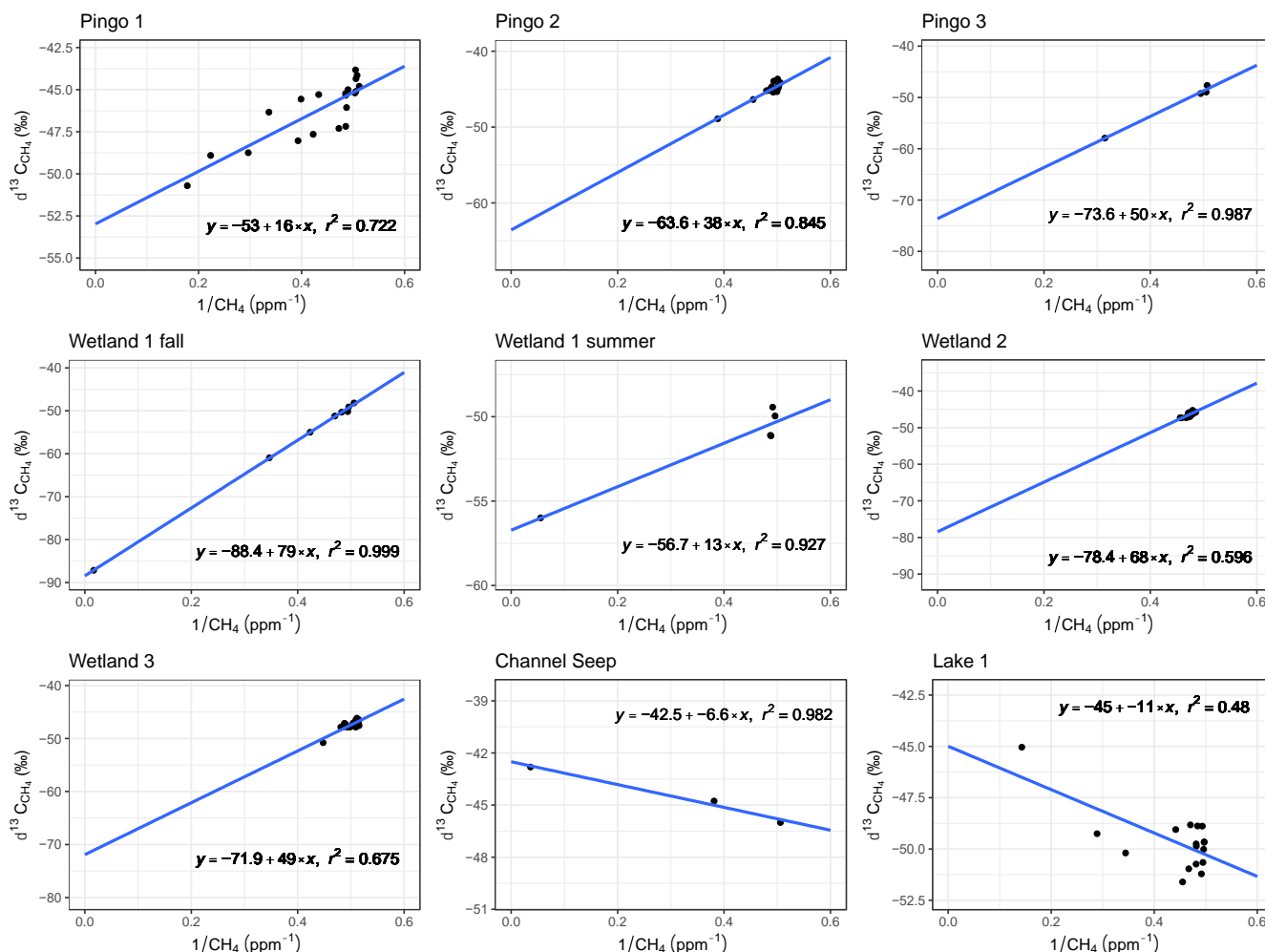


Channel Seep: A very active seep in a river channel observed during a previous field campaign. Samples were collected by extending the sample inlet on a pole over the channel and taking subsequent samples further away from the channel. No walking transects were collected at this site.



Lake 1: A large lake with prominent ebullition. During summer sampling, discrete samples were collected over the water by boat and along the shore downwind of the lake. Flux chamber measurements were taken near the lakeshore. No walking transects were taken at this site. Field of view is approximately 250 m wide.

**Figure 2: Site Pictures. Pingo 1, Pingo 2, Wetland 2 and Wetland 3 were identified as hotspots of methane production during aerial surveys by Kohnert et al. (2017). Pingo 3, Wetland 1 and Lake 1 were identified by holes in the ice forming on water bodies caused by high rate CH<sub>4</sub> ebullition. Channel Seep was identified by anomalously high CH<sub>4</sub> ebullition spotted from a helicopter during the summer. Pingo 1, Pingo 3, Wetland 1 and Lake 1 were sampled twice each, once during summer and once during the fall. Photo credit: Roger MacLeod, James Zheng.**



525 **Figure 3: Keeling plots for Pingo 2, Wetland 3, Pingo 1, Wetland 2, Channel Seep, Lake 1, Wetland 1 and Pingo 3. Source signatures ranged from -42 to -88 ‰  $\delta^{13}\text{C}_{\text{CH}_4}$ , which includes both thermogenic to biogenic signatures. Channel Seep and Lake 1 had thermogenic signatures, Pingo 3, Wetland 1, Wetland 2 and Wetland 3 had biogenic signatures while Pingo 1 and Pingo 2 had signatures which indicate a mixture of thermogenic and biogenic  $\text{CH}_4$ . The grey region indicates the 95% confidence interval of the regression line.**



530 **Table 1: Mean values of CH<sub>4</sub> and CO<sub>2</sub> determined from statistics for walking transects. Elevated CH<sub>4</sub> was measured at all sites but concentrations at Pingo 1, Pingo 2, and Wetland 1 were much higher than the other three. Elevated CO<sub>2</sub> was observed at Wetland 2, Pingo 2, Pingo 3 and Wetland 1.**

<b>CH<sub>4</sub> (ppm)</b>						
<b>Site</b>	<b>Pingo 1</b>	<b>Pingo 2</b>	<b>Pingo 3</b>	<b>Wetland 1</b>	<b>Wetland 2</b>	<b>Wetland 3</b>
mean	3.047	2.479	2.045	2.596	2.093	1.980
median	2.655	1.972	2.040	2.256	2.109	1.950
min	1.971	1.676	1.974	2.061	1.628	1.707
max	6.135	8.734	2.946	12.399	2.152	2.264
sd	0.955	1.479	0.039	1.049	0.071	0.107
<b>CO<sub>2</sub> (ppm)</b>						
<b>Site</b>	<b>Pingo 1</b>	<b>Pingo 2</b>	<b>Pingo 3</b>	<b>Wetland 1</b>	<b>Wetland 2</b>	<b>Wetland 3</b>
mean	389	402	416	415	430	391
median	389	393	413	413	413	393
min	380	359	380	406	342	361
max	396	462	519	488	603	400
sd	5	21	9	8	43	7
wind speed (km/h)	5.5	10.5	3.6	5.0	10.0	6.0